Spectral classification of coupling regimes in the quantum Rabi model

Daniel Z. Rossatto,[1,*] Celso J. Villas-Bôas,[1] Mikel Sanz,[2,†] and Enrique Solano[2,3]
[1]*Departamento de Física, Universidade Federal de São Carlos, 13565-905, São Carlos, SP, Brazil*
[2]*Department of Physical Chemistry, University of the Basque Country UPV/EHU, Apartado 644, E-48080 Bilbao, Spain*
[3]*IKERBASQUE, Basque Foundation for Science, María Díaz de Haro 3, E-48013 Bilbao, Spain*
(Received 20 December 2016; published 24 July 2017)

The quantum Rabi model is in the scientific spotlight due to the recent theoretical and experimental progress. Nevertheless, a full-fledged classification of its coupling regimes remains as a relevant open question. We propose a spectral classification dividing the coupling regimes into three regions based on the validity of perturbative criteria on the quantum Rabi model, which allows us the use of exactly solvable effective Hamiltonians. These coupling regimes are (i) the perturbative ultrastrong coupling regime which comprises the Jaynes-Cummings model, (ii) a region where nonperturbative ultrastrong and nonperturbative deep strong coupling regimes coexist, and (iii) the perturbative deep strong coupling regime. We show that this spectral classification depends not only on the ratio between the coupling strength and the natural frequencies of the unperturbed parts, but also on the energy to which the system can access. These regimes additionally discriminate the completely different behaviors of several static physical properties, namely the total number of excitations, the photon statistics of the field, and the cavity-qubit entanglement. Finally, we explain the dynamical properties which are traditionally associated with the deep strong coupling regime, such as the collapses and revivals of the state population, in the frame of the proposed spectral classification.

DOI: 10.1103/PhysRevA.96.013849

I. INTRODUCTION

The well-established Rabi model [1] describes the simplest class of light-matter interaction, the dipolar coupling between a two-level quantum system (qubit) and a classical monochromatic radiation field (unidimensional harmonic oscillator). In its quantum version, the radiation is specified by a quantized single-mode field, yielding the so-called quantum Rabi model (QRM) [2,3]. This model accurately describes the dynamics of a wide variety of physical setups, ranging from quantum optics to condensed matter systems [4]. In addition, a plethora of protocols in contemporary quantum information theory [5], with potential applications in future quantum technologies covering from ultrafast gates [6] to quantum error correcting codes [7] or remote entanglement generation [8,9], make use of the QRM as a building block. Therefore, the QRM plays an extremely important role in both theoretical and applied physics.

Typically, the standard experiments on cavity quantum electrodynamics (cavity QED) are restricted to a light-matter coupling strength much smaller than the natural frequencies of the unperturbed parts. Thus, they happen in the realm of the renowned Jaynes-Cummings (JC) model [10], which is obtained by applying the rotating-wave approximation (RWA) to the QRM [11]. In this scenario, the achievement of the so-called strong coupling (SC) regime, when the coupling strength exceeds all decoherence rates, has driven the field of cavity QED for several decades [4]. Therefore, the JC model has served as a theoretical and experimental milestone in the history of quantum physics.

Since the last decade, a new coupling regime of the QRM, in which the coupling strength is a substantial fraction of the natural frequencies of the unperturbed parts, is being theoretically studied [12–18] and experimentally reached in diverse solid state systems [18–32]. In this so-called ultrastrong coupling (USC) regime, the RWA is no longer suitable, such that the counter-rotating terms provide novel counterintuitive physical phenomena and new applications for the QRM emerge [6–9,33–44]. When the counter-rotating terms can still be perturbatively treated, as in Refs. [18–30], the QRM is approximately described by the Bloch-Siegert (BS) Hamiltonian [14,19,45]. However, a few experiments have recently achieved the nonperturbative USC regime [46–50], for which the full QRM has to be considered.

When the coupling strength is even stronger, surpassing the natural frequencies of the unperturbed parts, another regime of light-matter interaction appears, with totally different physics than the USC regime [51,52]. For this so-called deep strong coupling (DSC) regime [51], the QRM can be reasonably described by an approximate solution as discussed in Refs. [51,53–60]. And, recently, Yoshihara *et al.* have experimentally achieved such an impressive coupling in superconducting circuits [49,50].

Therefore, the advent of the aforementioned remarkable experimental and theoretical achievements has placed the QRM in the scientific spotlight. Nonetheless, the characterization so far established for the coupling regimes of the QRM is not quite universal, and a more specific criterion still remains undetermined. For instance, there are definitions stating that the USC regime is reached when the coupling strength is greater than a critical value related to either dynamical correlation functions [61] or quantum phase transitions [62,63]. However, for the latter case there is no consensus whether this transition can be reached in physical setups [63–67], and this definition does not take into account the properties of the whole model, but only of its ground state, where this limitation is also presented in Ref. [68]. Another attempt was recently proposed in Ref. [50], where the coupling classification is based on unique features exhibited in the transmission

*zini@df.ufscar.br
†mikel.sanz@ehu.eus

spectra of the system for different coupling regions. This approach uses the fact that the selection rules which allow or forbid transitions between eigenstates depend on the coupling value, changing the transmission pattern for different coupling regions. However, similarly to Refs. [62,63,68], this approach does not take into account the properties of the whole model, since only the first four eigenstates are considered.

On the other hand, it is also conjectured in the literature that the USC regime is achieved when the coupling strength is just a substantial fraction of the natural frequencies of the unperturbed systems [13,18–21]. Here, we are interested in quantitatively establishing how substantial this fraction has to be for the system description being significantly affected by the counter-rotating terms. Although the exact analytical solution of the QRM was recently presented for all parameter regimes [2], it strongly depends on zeros of a transcendental function defined through an infinite power series, making it difficult to extract the fundamental physics of that solution in general. Hence, it is more convenient to use approximate versions of the QRM as far as possible.

In this paper, we show that these approximate solutions are excellent guides to define a quantitative characterization of the coupling regimes of the QRM. In Sec. II, we show that the coupling regimes are naturally divided into three regions, whose boundaries depend not only on the ratio between the coupling strength and the natural frequencies of the unperturbed parts, but also on the energy to which the system can access. In addition, we show in Sec. III that our classification is supported by a completely different behavior of several static physical properties of the QRM, which depends on the region. Section IV provides a connection of our spectral classification with the dynamical properties that yield the traditionally blurry transition between the USC and DSC regimes. Finally, Sec. V comprises the conclusions of our work and the novel open questions emerging from it.

II. COUPLING REGIMES OF THE QUANTUM RABI MODEL

The Hamiltonian of the ubiquitous QRM is ($\hbar = 1$)

$$H_R = \omega a^\dagger a + \frac{\Omega}{2}\sigma_z + g_0\sigma_x(a + a^\dagger). \tag{1}$$

Here, $\sigma_{x,y,z}$ are the Pauli matrices for the qubit, with transition frequency Ω ($|\mathrm{g}\rangle$ = ground state and $|\mathrm{e}\rangle$ = excited state), and a ($a^\dagger$) stands for the annihilation (creation) operator of a single-mode bosonic field, with frequency ω. The light-matter coupling is quantified by the vacuum-Rabi frequency g_0.

A. Perturbative ultrastrong coupling regime

Whenever $|\delta| \ll g_0\sqrt{\langle\hat{n}\rangle + 1} \ll \Sigma$, with $\delta = \Omega - \omega$, $\Sigma = \Omega + \omega$, and $\langle\hat{n}\rangle = \langle a^\dagger a\rangle$, the QRM is well described by the JC model using the RWA [11],

$$H_{\mathrm{JC}} = \omega a^\dagger a + \frac{\Omega}{2}\sigma_z + g_0(a\sigma_+ + a^\dagger\sigma_-), \tag{2}$$

with $\sigma_\pm = (\sigma_x \pm i\sigma_y)/2$. Paradigmatic examples of the intuitive physics behind the JC dynamics are the Rabi oscillations in the JC doublets, Eqs. (9) and (10) with $\omega_{\mathrm{BS}} = g_0^2/\Sigma \to 0$, as a consequence of the conservation of the total number of excitations, and the collapses and revivals of the population inversion of the qubit [11].

When the counter-rotating terms can still be perturbatively treated, it is convenient to use the unitary transformation,

$$\mathcal{U} = \exp\left(\Lambda(a\sigma_- - a^\dagger\sigma_+) + \xi(a^2 - a^{\dagger 2})\sigma_z\right), \tag{3}$$

with $\Lambda = g_0/(\omega + \Omega)$ and $\xi = g_0\Lambda/2\omega$. To second order in Λ, this yields the Bloch-Siegert (BS) Hamiltonian [14,19,45],

$$\mathcal{U}^\dagger H_R \mathcal{U} \approx H_{\mathrm{BS}}^{(2)} = \omega_{\mathrm{BS}}\sigma_z a^\dagger a + \omega_{\mathrm{BS}}\frac{\sigma_z}{2} - \frac{\omega_{\mathrm{BS}}}{2} + H_{\mathrm{JC}}, \tag{4}$$

in which $\omega_{\mathrm{BS}} = g_0^2/\Sigma$ is the BS shift. From Eq. (4), it is straightforward to note that while the BS Hamiltonian provides the second-order correction in Λ, the JC provides the zeroth-order one. Hence, the JC model is recovered from the BS Hamiltonian by imposing $\Lambda = 0 \Rightarrow \omega_{\mathrm{BS}} = 0$.

The energy spectrum of the BS Hamiltonian is

$$E_0^{\mathrm{BS}} = -\frac{\Omega}{2} - \omega_{\mathrm{BS}}, \tag{5}$$

$$E_{n,\pm}^{\mathrm{BS}} = \left(n - \frac{1}{2}\right)\omega - \omega_{\mathrm{BS}} \pm \frac{1}{2}\sqrt{\left(\Delta_n^{\mathrm{BS}}\right)^2 + 4g_0^2 n}, \tag{6}$$

with $\Delta_n^{\mathrm{BS}} = \delta + 2\omega_{\mathrm{BS}}n$ and $n \in \mathbb{N}^*$. The eigenstates are

$$\left|\phi_0^{\mathrm{BS}}\right\rangle = \mathcal{U}|\mathrm{g},0\rangle, \tag{7}$$

$$\left|\phi_{n,\pm}^{\mathrm{BS}}\right\rangle = \mathcal{U}|\pm,n\rangle, \tag{8}$$

with $|\mathrm{g},n\rangle = |\mathrm{g}\rangle \otimes |n\rangle$, where $|n\rangle$ is the Fock state, and

$$|+,n\rangle = \cos\frac{\theta_n}{2}|\mathrm{e},n-1\rangle + \sin\frac{\theta_n}{2}|\mathrm{g},n\rangle, \tag{9}$$

$$|-,n\rangle = \sin\frac{\theta_n}{2}|\mathrm{e},n-1\rangle - \cos\frac{\theta_n}{2}|\mathrm{g},n\rangle, \tag{10}$$

in which the BS mixing angle is

$$\theta_n = \arctan\left(\frac{2g_0\sqrt{n}}{\Delta_n^{\mathrm{BS}}}\right). \tag{11}$$

For the sake of simplicity, we will consider the resonant case ($\omega = \Omega$) hereafter, but it is worth stressing that the following discussion is also suitable for the general case. In Fig. 1, we observe that the BS Hamiltonian provides an energy spectrum in excellent agreement with the one of the full QRM [69], surprisingly up to the first energy-level crossings (the so-called Juddian points [2]). Even though the BS Hamiltonian provides a second-order correction, this approximation breaks down around the paired-level first cross as also happens for the RWA, which is qualitatively pointed out in Refs. [54,55]. In the following we investigate this approximation in detail, being able to show quantitatively the validity of the BS Hamiltonian as a function of both the coupling and the energy of the system.

Therefore, the use of the first Juddian points is an excellent attempt to define a boundary for a coupling regime. In this case, since the BS Hamiltonian perturbatively takes into account the breakdown of the RWA, we can establish the *perturbative USC regime* (pUSC) of the QRM as the region before the first Juddian points ($g_{\mathrm{pUSC}}^{\times}$), which is obtained by imposing

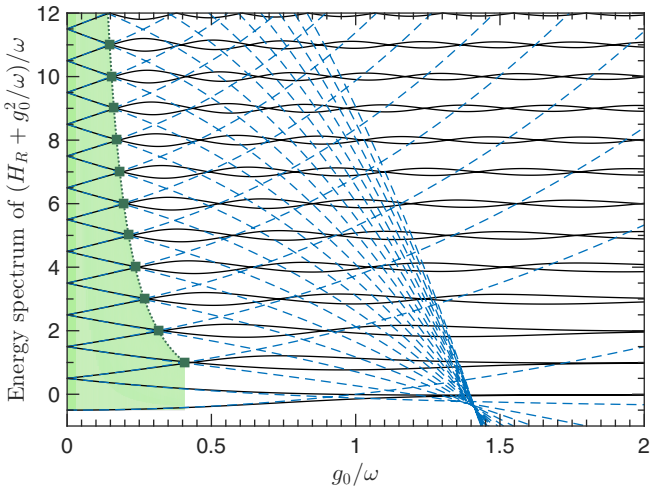

FIG. 1. Energy spectrum of the QRM (solid lines) and BS energy spectrum (dashed lines) vs g_0/ω. The squares represent the first Juddian points calculated using Eq. (12), while the shaded area is the region where the perturbative USC regime is valid [Eq. (14)]. For the sake of clarity, the eigenenergies are rescaled by g_0^2/ω.

$E^{\rm BS}_{n,+} = E^{\rm BS}_{n+1,-}$. By squaring both sides of $E^{\rm BS}_{n,+} = E^{\rm BS}_{n+1,-}$ up to the elimination of the square roots, we end up with an eighth-degree polynomial in g_0/ω. Since the BS Hamiltonian is valid for perturbative values of g_0/ω, we truncate this polynomial up to second order, so that its non-negative solution yields the first Juddian points for each $n \geqslant 1$,

$$\frac{g^{\times}_{\rm pUSC}}{\omega} \simeq \frac{1}{\sqrt{2(2n+1)}}, \tag{12}$$

such that $0 \leqslant g^{\times}_{\rm pUSC}/\omega \lesssim 1/\sqrt{6}$.

We can also notice from Fig. 1 that the more energetic the eigenenergies, the smaller the coupling values of first the Juddian points. This indicates that the importance of the counter-rotating terms depends not only on the ratio g_0/ω, but also on the energy to which the system can access, showing that the properties of the ground state are not sufficient to fully classify the coupling regimes of the QRM. Thus, the definition of the pUSC coupling regime is also connected to the energy to which the system can access.

Let us enlarge upon this point for the sake of clarity. The question we want to answer is whether a quantum state $|\psi\rangle$ evolving under H_R with a given g_0/ω will show features corresponding to the pUSC regime. This state is not necessarily an eigenstate, but it may be expanded in terms of eigenstates of the QRM. Thus, for a given g_0/ω, $|\psi\rangle$ can have contributions from eigenstates in the pUSC region and from the region beyond that. Therefore, we take as a natural qualitative quantifier the mean energy of the state $\bar{\mathcal{E}} = \langle\psi|H_R|\psi\rangle$ and choose the criterion that this state is in the pUSC regime when its energy is below the curve shown in the following.

If we invert Eq. (12) and replace n in $E^{\rm BS}_{n,+}$, assuming it as a continuous parameter, we can define the boundary of the pUSC regime as

$$\frac{\mathcal{E}_{\rm pUSC}}{\omega} \simeq \frac{1}{4}\left(\frac{\omega}{g_0}\right)^2\left[1-2\left(\frac{g_0}{\omega}\right)^4\right] - 1 + \frac{1}{4}\sqrt{\left[5-2\left(\frac{g_0}{\omega}\right)^2\right]\left[1-2\left(\frac{g_0}{\omega}\right)^2\right]}. \tag{13}$$

This boundary is illustrated as the dotted line in Fig. 1, with the shaded area standing for the region where the perturbative USC regime is valid, i.e., when

$$g_0 \lesssim g^{\times}_{\rm pUSC} \quad \text{and} \quad \bar{\mathcal{E}} \lesssim \mathcal{E}_{\rm pUSC}. \tag{14}$$

It is worth stressing that, besides the BS approach, there are other ones that can describe more accurately the QRM in a perturbative way [53–60]. However, these methods result in a much more complicated solution for $g^{\times}_{\rm pUSC}$. We have also checked that the BS Hamiltonian expanded to third order in g_0/ω [43] provides more accurate eigenenergies, which also diverge from the exact calculated ones beyond the first Juddian points (see Appendix A). This indicates that the proposed definition for the pUSC region is not a simple consequence of the second-order term, but something deeper related to the breaking of the assumptions for the adiabatic expansion and the point from which the total number of excitation is no longer preserved, as discussed in Sec. III and shown in the left panel of Fig. 4(a).

Considering the nonresonant case, our method can be straightforwardly applied to the cases that are not far of resonance ($\Omega \sim \omega$). For $\Omega \geqslant 2\omega$, the first-level crossings, predicted by the BS Hamiltonian, occur for $E^{\rm BS}_{n,+} = E^{\rm BS}_{n+p,-}$, where p is the integer part of the ratio Ω/ω. When p is even, the BS Hamiltonian wrongly predicts first crossings, because, in fact, the QRM has anticrossings instead. However, the BS Hamiltonian still satisfactorily reproduces the QRM before these first-level anticrossings. For extremely large detunings, better results are obtained by using effective Hamiltonians that also take into account either $\Omega \ll \omega$ [53–60] or $\Omega \gg \omega$ [70] in their derivations. However, for those cases a clear solution for both $g^{\times}_{\rm pUSC}$ and $\mathcal{E}_{\rm pUSC}$ may not be available.

B. Perturbative deep strong coupling regime

Analogously to the previous case, we can also employ the same ideas for the coupling regime at the other end, i.e., when the interaction term is no more a mere perturbation, but the main driver of the dynamics (DSC regime). In order to visualize the essence of this regime, it is convenient to rewrite H_R in terms of the parity operator $\Pi = -\sigma_z(-1)^{a^\dagger a}$ [51], a conserved quantity of the QRM besides the total energy [2],

$$H_R = \omega b^\dagger b + g_0(b + b^\dagger) - \frac{\Omega}{2}(-1)^{b^\dagger b}\Pi, \tag{15}$$

with $b = \sigma_x a$. Since Π has eigenvalues $p = \pm 1$ and $[\Pi, H_R] = 0$, there exists an independent Hamiltonian describing a perturbed displaced harmonic oscillator for each parity chain ($p = \pm 1$), whose perturbation is given by the qubit term as an energy shift proportional to Ω [51]. Thus, a perturbative approach up to first order in Ω provides the following energy spectrum and the zeroth-order eigenstates

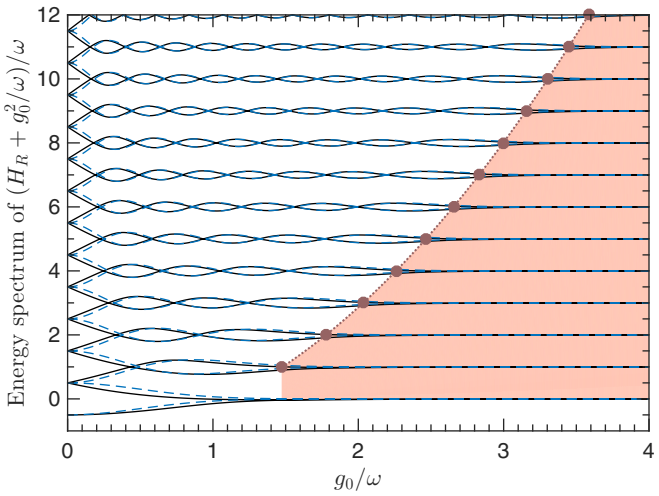

FIG. 2. Comparison between the energy spectrum of the QRM (solid lines) and the adiabatic approximation (dashed lines) given by Eq. (16), with the circles representing the first solutions of Eq. (18) for $\epsilon = 0.1$ (Table I). The shaded area is the region where the perturbative DSC regime is valid [Eq. (20)]. For the sake of clarity, the eigenenergies are rescaled by g_0^2/ω.

(adiabatic approximation) [51,53–60],

$$E_{\pm,n}^{\mathrm{pDSC}} = (n-\alpha^2)\omega \pm \frac{\Omega}{2} e^{-2\alpha^2} L_n(4\alpha^2), \tag{16}$$

$$\left|\phi_{\pm,n}^{\mathrm{pDSC}}\right\rangle = \frac{1}{\sqrt{2}}[|+\rangle \otimes \mathcal{D}(-\alpha)|n\rangle \pm |-\rangle \otimes \mathcal{D}(\alpha)|n\rangle], \tag{17}$$

in which $L_n(x)$ is the Laguerre polynomial, $|\pm\rangle = (|\mathrm{e}\rangle \pm |\mathrm{g}\rangle)/\sqrt{2}$, $\mathcal{D}(\alpha) = e^{\alpha a^\dagger - \alpha^* a}$ with $\alpha = g_0/\omega$, and $n \in \mathbb{N}$. The energy of the ground state for this case is given by $E_{0,-}^{\mathrm{pDSC}}$. A more refined approximation improves only marginally the accuracy of the eigenenergies and does not reveal new physical behavior [61].

The DSC regime has a typical dynamical feature, which is the appearance of photon-number wave packets that bounce back and forth along a defined parity chain, yielding collapses and revivals of the initial population, even when the field and the qubit are initially in the vacuum and ground state, respectively [51]. This feature appears only for sufficient large values of g_0/ω, and it is more prominent after the last Juddian points (last energy-level crossings), when the adjacent eigenenergies asymptotically approach, becoming quasidegenerate. Notice that the spectrum and the eigenstates of the QRM are described by Eqs. (16) and (17) with high fidelity [61]. Therefore, it is straightforward to note that the collapse-revival phenomenon is strictly related to the Schrödinger-cat-like states given by Eq. (17), which makes the perturbative solution an excellent attempt to define a boundary for a coupling regime.

In Fig. 2, considering $\omega = \Omega$, we notice that the energy spectrum given by Eq. (16) strongly agrees with the one of the full QRM beyond the last Juddian points, when the adjacent eigenenergies become quasidegenerate. Thus, we use this fact to establish the boundary delimiting the *perturbative DSC* (pDSC) region. The boundary also connects

TABLE I. First numerical solutions of Eq. (18) for a $\epsilon = 0.1$.

n	$g_{\mathrm{pDSC}}^{\times}/\omega$	n	$g_{\mathrm{pDSC}}^{\times}/\omega$
1	1.473	7	2.832
2	1.778	8	2.998
3	2.035	9	3.155
4	2.261	10	3.304
5	2.466	11	3.447
6	2.655	12	3.584

with the appearance of the collapse and revivals of the initial population. For this purpose, let us consider the set of $\alpha_k(n,\epsilon)$, with $n \geqslant 1$ and $k = 1,2,\ldots,m \leqslant n$, which are solutions of the equation,

$$\frac{1}{\omega}\left|E_{+,n}^{\mathrm{pDSC}} - E_{-,n}^{\mathrm{pDSC}}\right| = e^{-2\alpha^2}|L_n(4\alpha^2)| \equiv \epsilon, \tag{18}$$

where ϵ is the maximum allowed energy difference close to the quasidegenerate-energy region, which is related to the minimum fidelity allowed between the exact solution of the QRM and the perturbative states $|\phi_{\pm,n}^{\mathrm{pDSC}}\rangle$. For a given n and ϵ, Eq. (18) can have at maximum n solutions (indexed by k), since it is a transcendental equation involving a Laguerre polynomial of order n with an exponential envelope. Therefore, since we are interested in the quasidegenerate-energy region beyond the last Juddian points (related to the largest roots of the Laguerre polynomials), the limit of the pDSC region is given by the set of largest solutions of the above transcendental equation, i.e., for a given n and ϵ, we have $g_{\mathrm{pDSC}}^{\times}/\omega = \max_k[\alpha_k(n,\epsilon)]$.

For our calculations, we have chosen $\epsilon = 0.1$, value for which we have numerically observed better than 99% fidelity between $|\phi_{\pm,n}^{\mathrm{pDSC}}\rangle$ and the corresponding exact eigenstates of the QRM. The numerical solutions of Eq. (18) corresponding to the lowest values of n are provided in Table I. Inserting $g_{\mathrm{pDSC}}^{\times}$ into $(E_{+,n}^{\mathrm{pDSC}} + E_{-,n}^{\mathrm{pDSC}})/2$, these points can be accurately fitted by the second-order equation,

$$\frac{\mathcal{E}_{\mathrm{pDSC}}}{\omega} \simeq a\left(\frac{g_0}{\omega}\right)^2 + b\left(\frac{g_0}{\omega}\right) + c, \tag{19}$$

with $a = 0.0425$, $b = -0.054478$, and $c = -1.1987$, which is our definition of the boundary of the pDSC regime. Such a boundary is illustrated as the dotted line in Fig. 2, with the shaded area indicating the region where the perturbative DSC regime is valid, i.e., when

$$g_0 \gtrsim g_{\mathrm{pDSC}}^{\times} \quad \text{and} \quad \bar{\mathcal{E}} \lesssim \mathcal{E}_{\mathrm{pDSC}}. \tag{20}$$

If we change $\epsilon \to \epsilon + \Delta\epsilon$ (with $|\Delta\epsilon| \ll |\epsilon|$), the new solution of the transcendental equation will be simply $\alpha = \alpha_\epsilon + \lambda\Delta\epsilon$, with

$$\lambda = -\frac{e^{2\alpha_\epsilon^2}}{4\alpha_\epsilon\left(L_n\left(4\alpha_\epsilon^4\right) + 2L_{n-1}^1\left(4\alpha_\epsilon^2\right)\right)}, \tag{21}$$

where α_ϵ is the solution for ϵ.

It is noteworthy to mention that we have numerically observed that the last maximum of the function $e^{-x/2}|L_n(x)|$ is monotonically decreasing with n. As a consequence, it could be that, for any fixed ϵ, there exists a value of n such that the last solution to Eq. (18) could be placed before the last

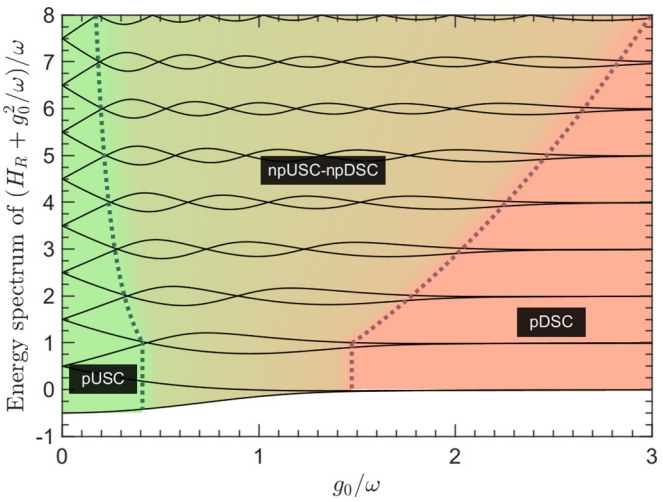

FIG. 3. Classification of the coupling regimes of the QRM. The region before the first Juddian points stands for the perturbative ultrastrong coupling (pUSC) regime, while the region beyond the last Juddian points represents the perturbative deep strong coupling (pDSC) regime. The intermediate region symbolizes the nonperturbative ultrastrong–deep strong coupling (npUSC-npDSC) regime. The color gradient around the boundaries symbolizes that our spectral classification does not imply an abrupt change in the physical properties of the QRM. Actually, such changes occur gradually, as shown in Secs. III and IV.

Juddian point. In any case, even in the situation in which this does not hold or when we want ϵ above this threshold, there are several strategies to overcome this complication. The most straightforward approach is to consider the analytical extension of the curve fitted for smaller n. This actually works since this region is indeed perturbative. A second more complicated approach is introducing $\epsilon = 1 - F$, with F the fidelity of the perturbative eigenstates given by Eq. (17) in comparison with the exact eigenstates of the QRM. The problem with this approach relies on the lack of an analytically simple expression for the exact eigenstates of the QRM, and thus the fidelity can only be calculated numerically.

For the nonresonant case, our definition of the pDSC regime can also be extended to the near-resonant case straightforwardly. When $\Omega \ll \omega$ the solution given by Eqs. (16) and (17) is still very suitable, but for $\Omega \gg \omega$ such solution does not provide a good fidelity and a solution that directly consider such a limit in its derivation is required [70]. However, the procedure to define the pDSC region remains the same.

C. Nonperturbative ultrastrong–deep strong coupling regime

According to the aforementioned results, we are able to classify the coupling regimes of the QRM into three regions, whose boundaries depend not only on the relation between the coupling strength and the natural frequencies of the unperturbed parts, but also on the mean energy that the system can access, as summarized in Fig. 3. The pUSC regime belongs to the region right before the first Juddian points, whose physics are well described by the BS Hamiltonian, which still considers the interaction term as a perturbation. The BS Hamiltonian includes the well-known JC model, i.e., the QRM under the RWA. On the other hand, the pDSC regime belongs to the region beyond the last Juddian points, where there is a role interchange, since the interaction Hamiltonian becomes the main driver of the dynamics, while the bare Hamiltonian is the perturbative term. Finally, between these two coupling regimes, there is a region in which all parts of the Hamiltonian contribute on an equal footing to the dynamics. Then, we can establish this region as the nonperturbative USC (npUSC) regime, or as the nonperturbative DSC (npDSC) regime.

III. STATIC PROPERTIES

Although our classification seems originally related to the validity of approximate mathematical models, it is associated with physical properties of the QRM which change their behavior qualitatively from region to region. In this section, we will focus on three relevant static properties, namely, the total number of excitations in the system, the photon statistics of the field, and the cavity-qubit entanglement.

In Fig. 4(a), we show the total number of excitations ($n_e = \langle \hat{n}_e \rangle = \langle a^\dagger a + \sigma_+ \sigma_- \rangle$) for each exact eigenstate of the QRM as a function of g_0/ω. In the left panel, we observe that the n_e remains almost unchanged for the lower-coupling region of the pUSC regime ($g_0 \ll g_{\mathrm{pUSC}}^{\times}$), which is expected since the BS Hamiltonian which governs the dynamics in this region commutes with $\hat{n}_e$. As we enter in the npUSC-npDSC regime, n_e has a nontrivial oscillatory dependency with the coupling strength, which ceases as we approach the pDSC region ($g_0 \sim g_{\mathrm{pDSC}}^{\times}$), as depicted in the right panel of Fig. 4(a). In the pDSC region, the total number of excitations becomes quasidegenerate and increases with $(g_0/\omega)^2$ for the higher-coupling region of this region, with $|n_e - (n + 1/2) - (g_0/\omega)^2| \leqslant \epsilon$ as shown in Appendix B. It is worth stressing that we have checked that n_e computed through the approximate eigenstates agrees very well with the one calculated via the exact eigenstates within the corresponding region. This is also true for the other physical quantities shown below, but we did not include such approximate results in Fig. 4 for the sake of clarity.

Another physical property with characteristic behavior in each coupling region is the photon statistics of the field. Using the Fano-Mandel parameter Q given by Eq. (C1) [11], we distinguish sub-Poissonian ($Q < 0$ − genuine nonclassical statistics), Poissonian ($Q = 0$), and super-Poissonian ($Q > 0$) statistics. Such characteristic behavior is illustrated in Fig. 4(b), where we note that, except for the first two eigenstates that do not have an energy crossing, the field always exhibits a sub-Poissonian and a super-Poissonian photon statistics in the pUSC and pDSC regimes (see Appendix C), respectively, while all kinds of photon statistics can be observed in the npUSC-npDSC regime. Moreover, we show in Appendix C that there are transitions in the photon statistics only in the npUSC-npDSC regime.

In Fig. 4(c), we observe that the entanglement between the qubit and the field (von-Neumann entropy of each subsystem [11]) also shows a peculiar behavior, with the minima only appearing in the npUSC-npDSC regime. In addition, each minimum is always localized between two Juddian points and

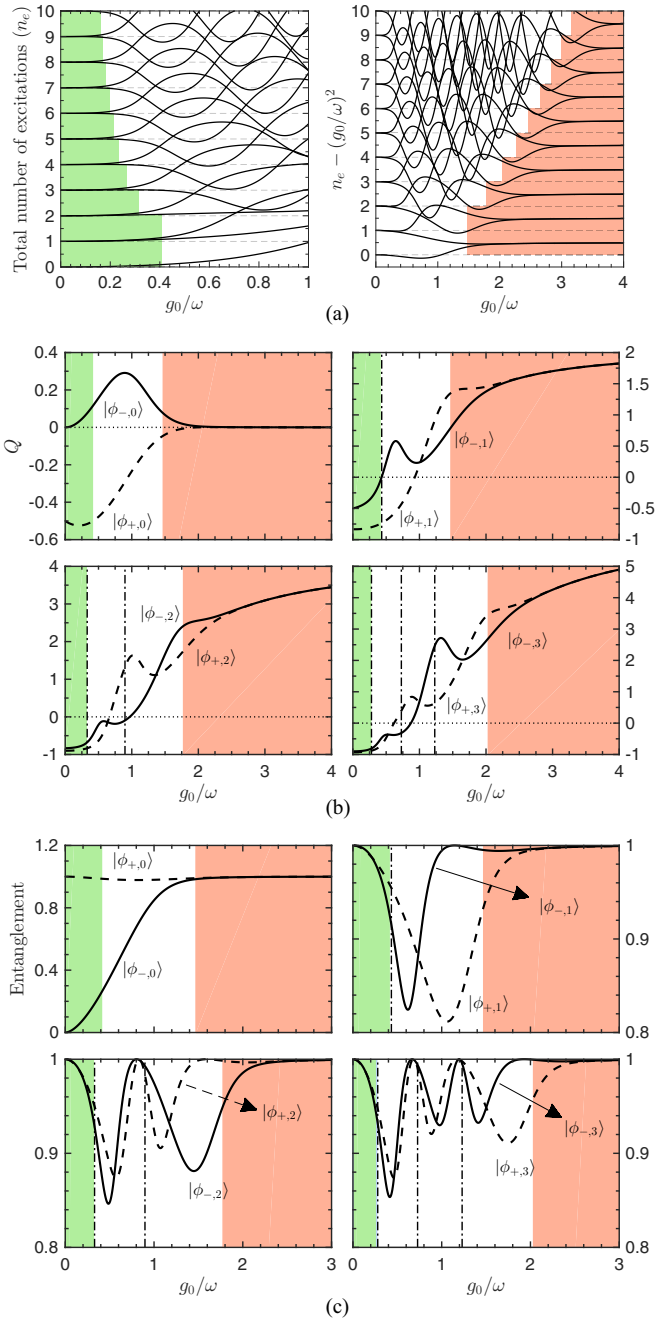

FIG. 4. (a) Total number of excitations, (b) Fano-Mandel parameter of the photon distribution of the field, and (c) qubit-field entanglement for the first exact eigenstates of the QRM in function of g_0/ω. The left and right shaded areas stand for the pUSC and pDSC regimes, respectively, while the vertical dashed-dotted lines stand for the energy crossings. For the sake of illustration, we use the same terminology of the pDSC regime to label the eigenstates in (b) and (c).

after the last one. The approximate analytical expressions of the qubit-field entanglement for the pUSC and pDSC regimes are given in Appendix D.

Our last remark is related to the decomposition of the field state in the Fock basis $\{|m\rangle\}$ for the higher-coupling region of the pDSC regime, i.e., for $g_0 \gg g_{\rm pDSC}^{\times}$. Using the

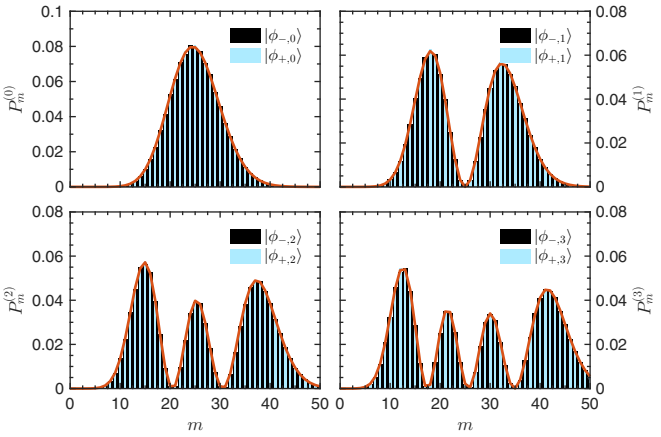

FIG. 5. Decomposition for $g_0 \gg g_{\rm pDSC}^{\times}$ of the field state in the Fock basis, considering $g_0 = 5\omega$. The bars are computed through the exact eigenstates, while the solid line is obtained by using Eq. (17).

terminology of the pDSC regime just to label the eigenstates, this decomposition is given by

$$P_m^{(\pm,n)} = \mathrm{Tr}(\mathbf{1}_q \otimes |m\rangle\langle m| \otimes |\phi_{\pm,n}\rangle\langle\phi_{\pm,n}|), \tag{22}$$

in which $\mathbf{1}_q = \sigma_+\sigma_- + \sigma_-\sigma_+$ and $\mathrm{Tr}(\bullet)$ is the trace operation. We display $P_m^{(\pm,n)}$ in Fig. 5 considering $g_0 = 5\omega$, in which we first recognize that $P_m^{(-,n)}$ and $P_m^{(+,n)}$ tend toward the same multimodal distribution centered at $m_c \simeq (g_0/\omega)^2$. This can be confirmed by using Eq. (17), which predicts (red solid line in Fig. 5)

$$P_m^{(\pm,n)} = \frac{\alpha^{2|m-n|}}{e^{\alpha^2}} \frac{\min(m,n)!}{\max(m,n)!} \left(L_{\min(m,n)}^{|m-n|}(\alpha^2)\right)^2, \tag{23}$$

in which $L_n^a(x)$ is the generalized Laguerre polynomial and $\alpha = g_0/\omega$. Secondly, we can also see that the number of modes of $P_m^{(\pm,n)}$, $n+1$, seems to be related to the number of energy crossings between $|\phi_{-,n}^{\rm pDSC}\rangle$ and $|\phi_{+,n}^{\rm pDSC}\rangle$, which is n.

It is worth emphasizing that the boundaries of our spectral classification does not imply an abrupt change in the physical properties of the QRM, as noticed in Fig. 4. Actually, such change gradually occurs around the boundaries of the pUSC and pDSC regions, even for dynamical properties as we will see in the next section.

IV. CONNECTION WITH DYNAMICAL PROPERTIES

As already mentioned in Sec. II B, the traditional characteristic signature of the DSC regime is not a static property, but a dynamical one—namely, the appearance of photon-number wave packets that bounce back and forth along a defined parity chain, yielding collapses and revivals of the initial population. In this section, we show how the appearance of this phenomenon is related to our spectral classification.

In the upper panel of Fig. 6, we show the spectral classification together with the mean energy $\langle\psi_0|H_R|\psi_0\rangle$ of two initial states, $|\mathrm{g},0\rangle$ (solid line) and $|\mathrm{g},1\rangle$ (dashed line), as function of g_0/ω. Considering the values of g_0 pointed out by the arrows, we computed the initial population $P_{|\psi_0\rangle} = \langle\psi_0|e^{-iH_R t}|\psi_0\rangle$. In the pUSC region, $P_{|\mathrm{g},0\rangle}$ remains almost constant since $|\mathrm{g},0\rangle$ is basically the ground state in that region

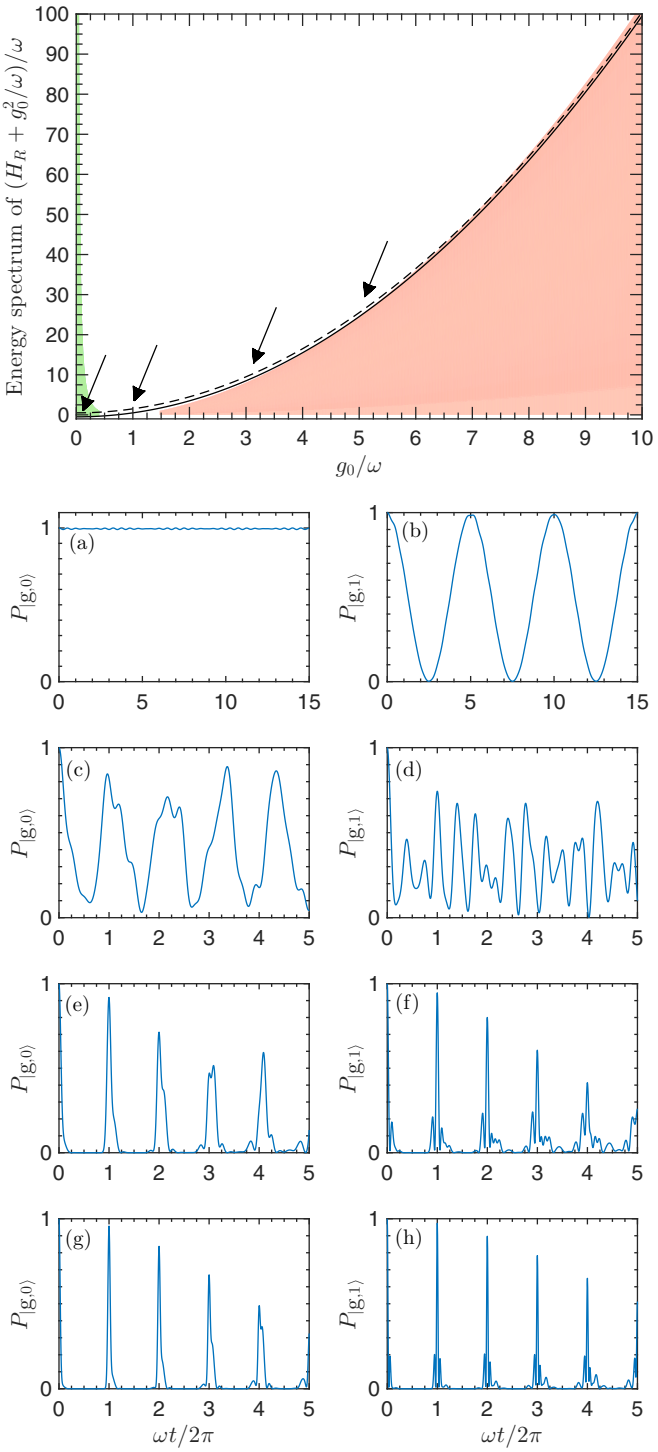

FIG. 6. (Upper panel) Spectral classification together with the mean energy of the initial states $|g,0\rangle$ (solid line) and $|g,1\rangle$ (dashed line) as function of g_0/ω. The arrows indicate the values of g_0 which are used for the computation of the initial population $P_{|g,0\rangle}$ and $P_{|g,1\rangle}$, namely, $g_0/\omega = 0.1$ in (a) and (b), $g_0/\omega = 1$ in (c) and (d), $g_0/\omega = 3$ in (e) and (f), and $g_0/\omega = 5$ in (g) and (h).

[Fig. 6(a)], while $P_{|g,1\rangle}$ exhibits Rabi oscillations due to the conservation of the total number of excitations [Fig. 6(b)]. As we enter in the npUSC-npDSC region, the Rabi oscillations pattern is lost, since the counter-rotating terms introduce a nontrivial oscillatory behavior in the initial population, as shown in Figs. 6(c) and 6(d). Finally, as we approach the pDSC region [Figs. 6(e) and 6(f)], the initial population starts to present the collapse-revival pattern, which becomes more prominent as we go inside that region [Figs. 6(g) and 6(h)].

V. CONCLUSION

In summary, we have introduced a spectral classification of the coupling regimes of the quantum Rabi model based on the validity of different perturbative approximations, showing that such regimes depend not only on the ratio between the coupling strength and the natural frequencies of the unperturbed parts, but also on the mean energy accessible by the system. Our classification comprises three coupling regions, namely the perturbative ultrastrong, the nonperturbative ultrastrong–deep strong, and the perturbative deep strong coupling regimes. Remarkably, we have shown that the spectral classification is supported by a clearly divergent behavior of several relevant static physical properties in different coupling regimes. Additionally, we have also tested the suitability of our classification for the usual dynamical properties studied in the literature, which yield the traditional vague USC-DSC division. Therefore, our results clearly answer the long-standing question of providing a founded comprehensible classification of the coupling regimes in the QRM. Moreover, our results also open novel questions which motivate further studies of the mathematical and physical properties of these coupling regions, such as the physical role of the Juddian points in the QRM.

ACKNOWLEDGMENTS

We thank D. Braak, S. Felicetti, G. Romero, J. Casanova, and P. Forn-Díaz for fruitful discussions. This work was supported by the São Paulo Research Foundation (FAPESP) Grants No. 2013/04162-5, No. 2013/23512-7, and No. 2014/24576-1, Brazilian National Institute of Science and Technology for Quantum Information (INCT-IQ), CNPq, Spanish MINECO/FEDER Grant No. FIS2015-69983-P, and Basque Government Grant No. IT986-16 and UPV/EHU Grant No. UFI 11/55.

APPENDIX A: INFLUENCE OF THE HIGHER ORDERS OF THE BS APPROXIMATION

In this Appendix, we discuss the influence of the third order of the BS expansion of the QRM in the definition of the pUSC region. First, let us consider the BS Hamiltonian expanded up to the third order in g_0/ω [43],

$$H_{\rm BS}^{(3)} = \omega a^\dagger a + \frac{\omega}{2}\sigma_z - \omega_{\rm BS}\left(\sigma_z a^\dagger a + \frac{1}{2}\right) + g(\hat{n})(a^\dagger\sigma^- + a\sigma^+), \tag{A1}$$

where

$$g(\hat{n}) = g_0\left(1 - a^\dagger a\frac{\omega_{\rm BS}}{2\omega}\right) \tag{A2}$$

is the photon-dependent coupling strength. Notice that the Hamiltonian given by Eq. (A1) preserves the number of excitations, i.e., $[H_{\rm BS}^{(3)}, a^\dagger a + \sigma_+\sigma_-] = 0$. In Fig. 7, the exact

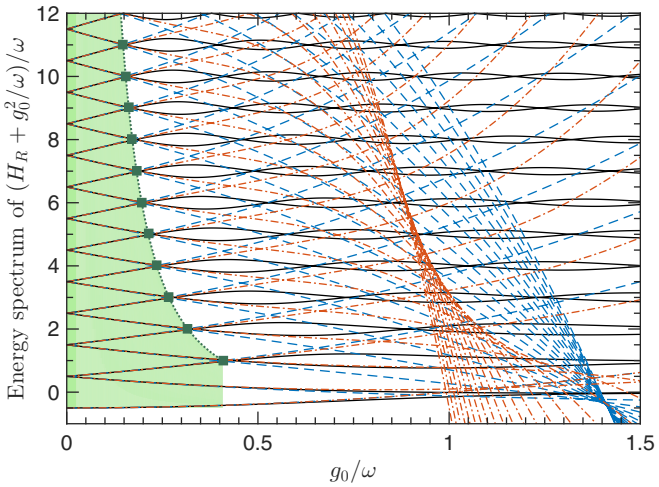

FIG. 7. Effect of the third-order BS expansion in the pUSC region. We compare the exact eigenenergies of the QRM (solid lines) with the eigenenergies of the second-order BS expansion (dashed lines) and the third-order BS expansion (dashed-dotted lines). We observe that the divergence is still in the first Juddian points, therefore the shaded region still stands for the pUSC regime.

eigenenergies of the QRM are depicted and compared with both the second and third orders of the BS expansion. One can observe that, even though the third order is more accurate, it still diverges from the correct eigenenergies also after the first Juddian points. Indeed, this will happen for any truncation in a finite order of the Bloch-Siegert expansion, because it corresponds to an adiabatic approximation. Hence, the increasing in the expansion order in the perturbation theory simply marginally improves the description before the Juddian points, points where the adiabatic approximation fails by definition because the gap closes. Therefore, the region of validity of the expansion cannot be enlarged by increasing the truncation order.

Thus, as mentioned in Sec. II A, the proposed definition for the pUSC region is not a simple consequence of the second-order term, but something deeper related to the breaking of the assumptions for the adiabatic expansion and the point from which the number of excitations starts to be not preserved, as we have seen in the left panel of Fig. 4(a). In addition, we see that the second-order expansion is enough to describe the physics that curiously lives before the first Juddian points.

APPENDIX B: TOTAL EXCITATIONS IN THE PERTURBATIVE REGIMES

The total number of excitations is given by the operator $\hat{n}_e = a^\dagger a + \sigma_+\sigma_-$. The fact that the number of excitations is preserved in the pUSC regime is a direct consequence of the commutation of this operator with the BS Hamiltonian $[\hat{n}_e, H_{\rm BS}^{(2)}] = 0$ (note that this also holds for $H_{\rm BS}^{(3)}$).

Let us now compute the mean value of the operator $\hat{n}_e$ in the pDSC regime, i.e., $\langle\hat{n}_e\rangle_{\rm pDSC} = \langle\phi_{\pm,n}^{\rm pDSC}|\hat{n}_e|\phi_{\pm,n}^{\rm pDSC}\rangle$. Hence,

$$\langle\hat{n}_e\rangle_{\rm pDSC} = \tfrac{1}{2}[\langle n|\mathcal{D}^\dagger(\alpha)a^\dagger a\mathcal{D}(\alpha)|n\rangle \pm \langle n|\mathcal{D}^2(\alpha)|n\rangle + 1 + \langle n|\mathcal{D}^\dagger(-\alpha)a^\dagger a\mathcal{D}(-\alpha)|n\rangle \pm \langle n|\mathcal{D}^2(-\alpha)|n\rangle], \tag{B1}$$

with $\alpha = g_0/\omega$. In order to compute the first term, we use $\langle n|\mathcal{D}^\dagger(x)a^\dagger a\mathcal{D}(x)|n\rangle = \langle n|(a^\dagger + x)(a + x)|n\rangle = n + x^2$. The second term is given by Eq. (D10), so that $\langle n|\mathcal{D}^2(x)|n\rangle = e^{-2x^2}{}_1F_1(-n,1;4x^2)$, in which ${}_1F_1(a,b;z)$ is the Kummer's confluent hypergeometric function. By using these functions real valued, we obtain

$$\begin{aligned}\langle\hat{n}_e\rangle_{\rm pDSC} - \alpha^2 &= n + \tfrac{1}{2} \pm e^{-2\alpha^2}{}_1F_1(-n,1;4\alpha^2)\\ &= n + \tfrac{1}{2} \pm \underbrace{e^{-2\alpha^2}L_n(4\alpha^2)}_{\leqslant\epsilon},\end{aligned} \tag{B2}$$

where we have made use of Kummer's transformation $L_n^{(\alpha)}(z) = \binom{n+\alpha}{n}{}_1F_1(-n,\alpha+1;z)$ [71]. Therefore, effectively, the variation in $\langle\hat{n}_e\rangle_{\rm pDSC} - \alpha^2$ is exponentially suppressed when $\alpha \to \infty$, and upper-bounded by ϵ in the pDSC region.

APPENDIX C: FANO-MANDEL PARAMETER IN PUSC AND PDSC

In this Appendix, we compute the photon statistics of the QRM eigenstates in the pUSC and pDSC regimes through the Fano-Mandel parameter,

$$Q = \frac{\langle\hat{n}^2\rangle - \langle\hat{n}\rangle^2}{\langle\hat{n}\rangle} - 1. \tag{C1}$$

Let us recall that the photon distribution is classified as sub-Poissonian ($Q < 0$ – genuine nonclassical statistics), Poissonian ($Q = 0$), and super-Poissonian ($Q > 0$).

1. Perturbative USC regime

First, we must compute the photon distributions of the eigenstates $|\phi_{n,\pm}^{\rm BS}\rangle$, which is defined by $P_m(\phi_{n,\pm}^{\rm BS}) = |\langle {\rm g},m|\phi_{n,\pm}^{\rm BS}\rangle|^2 + |\langle {\rm e},m|\phi_{n,\pm}^{\rm BS}\rangle|^2$. In order to perform the calculation, it is useful noticing that $\mathcal{U}^\dagger|{\rm g},m\rangle = \frac{1}{\sqrt{m!}}(\mathcal{U}^\dagger a^{\dagger m}\mathcal{U})\mathcal{U}^\dagger|{\rm g},0\rangle$, with $\mathcal{U}$ given by Eq. (3). By using the Baker-Campbell-Hausdorff formula to second order,

$$\mathcal{U}^\dagger a^m\mathcal{U} = a^m + [a^m,\mathcal{H}(\alpha)] + \tfrac{1}{2}[[a^m,\mathcal{H}(\alpha)],\mathcal{H}(\alpha)] + O(\alpha^3), \tag{C2}$$

with

$$\mathcal{H}(\alpha) = (\alpha/2)(a\sigma_- - a^\dagger\sigma+) + (\alpha^2/4)(a^2 - a^{\dagger 2})\sigma_z, \tag{C3}$$

and $\alpha = g_0/\omega$.

It is straightforward to prove the useful expressions $[a^\dagger,a^m] = -ma^{m-1}$ and $[a^{\dagger 2},a^m] = -m(a^\dagger a^{m-1} + a^{m-1}a^\dagger)$, which may be used to compute, to the second order, the commutator,

$$[a^m,\mathcal{H}(\alpha)] = -\frac{\alpha}{2}ma^{m-1}\sigma^\dagger - \frac{\alpha^2}{4}m\sigma_z(a^\dagger a^{m-1} + a^{m-1}a^\dagger) + O(\alpha^3). \tag{C4}$$

Let us now compute the second commutator of Eq. (C2) to the second order,

$$[[a^m,\mathcal{H}(\alpha)],\mathcal{H}(\alpha)] = -\frac{\alpha^2}{4}ma^m\sigma_z + O(\alpha^3). \tag{C5}$$

Therefore, by replacing Eqs. (C4) and (C5) into Eq. (C2), we obtain

$$\mathcal{U}^\dagger a^m\mathcal{U} = a^m - \frac{\alpha}{2}ma^{m-1}\sigma^\dagger - \frac{\alpha^2}{4}ma^m\sigma_z - \frac{\alpha^2}{4}m\sigma_z(a^\dagger a^{m-1} + a^{m-1}a^\dagger) + O(\alpha^3). \tag{C6}$$

Now, we have to compute $\mathcal{U}^\dagger|\mathrm{g},0\rangle$, also to the second order in α, i.e., $\mathcal{U}^\dagger = \mathbb{1} - \mathcal{H}(\alpha) + \frac{1}{2}\mathcal{H}(\alpha)^2 + O(\alpha^3)$, which yields after normalization,

$$\mathcal{U}^\dagger|\mathrm{g},0\rangle = \left(1 - \frac{\alpha^2}{8}\right)|\mathrm{g},0\rangle + \frac{\alpha}{2}|\mathrm{e},1\rangle - \frac{\alpha^2\sqrt{2}}{4}|\mathrm{g},2\rangle + O(\alpha^3). \tag{C7}$$

By using this together with Eq. (C2), we obtain

$$\mathcal{U}^\dagger|\mathrm{g},m\rangle = \left[1 - (m+1)\frac{\alpha^2}{8}\right]|\mathrm{g},m\rangle + \frac{\alpha}{2}\sqrt{m+1}|\mathrm{e},m+1\rangle - \frac{\alpha^2}{4}(\sqrt{(m+1)(m+2)}|\mathrm{g},m+2\rangle - \sqrt{m(m-1)}|\mathrm{g},m-2\rangle). \tag{C8}$$

Analogously,

$$\mathcal{U}^\dagger|\mathrm{e},m\rangle = \left(1 + m\frac{\alpha^2}{4}\right)|\mathrm{e},m\rangle - \frac{\alpha}{2}\sqrt{m}|\mathrm{g},m-1\rangle + \frac{\alpha^2}{4}(\sqrt{(m+1)(m+2)}|\mathrm{e},m+2\rangle - \sqrt{m(m-1)}|\mathrm{e},m-2\rangle). \tag{C9}$$

The scalar products of these states with respect to the state given by Eq. (9) yields

$$\langle \mathrm{g},m|\mathcal{U}|+,n\rangle = \left(1 + m\frac{\alpha^2}{4}\right)\cos\left(\frac{\theta_{m+1}}{2}\right)\delta_{n,m+1} - \frac{\alpha}{2}\sqrt{m}\sin\left(\frac{\theta_{m-1}}{2}\right)\delta_{n,m-1} + \frac{\alpha^2}{4}\left[\sqrt{(m+1)(m+2)}\cos\left(\frac{\theta_{m+3}}{2}\right)\delta_{n,m+3} - \sqrt{m(m-1)}\cos\left(\frac{\theta_{m-3}}{2}\right)\delta_{n,m-3}\right]. \tag{C10}$$

$$\langle \mathrm{e},m|\mathcal{U}|+,n\rangle = \left[1 - (m+1)\frac{\alpha^2}{8}\right]\sin\left(\frac{\theta_m}{2}\right)\delta_{n,m} + \frac{\alpha}{2}\sqrt{m+1}\cos\left(\frac{\theta_{m+2}}{2}\right)\delta_{n,m+2} - \frac{\alpha^2}{4}\left[\sqrt{(m+1)(m+2)}\cos\left(\frac{\theta_{m+2}}{2}\right)\delta_{n,m+2} - \sqrt{m(m-1)}\cos\left(\frac{\theta_{m-2}}{2}\right)\delta_{n,m-2}\right]. \tag{C11}$$

The sum of the squares of these elements gives the photon distributions $P_m(\phi^{\mathrm{BS}}_{n,+})$, for which we need to use the expressions $\sin^2\frac{\theta_n}{2} = \frac{1}{2}(1 - \frac{\alpha\sqrt{n}}{2})$ and $\cos^2\frac{\theta_n}{2} = \frac{1}{2}(1 + \frac{\alpha\sqrt{n}}{2})$.

Now, we want to compute the first and second moments of the distribution,

$$\langle\hat{n}\rangle = \sum_{m=0}^{\infty} m P_m^{+,n} = \left(n - \frac{1}{2}\right) - \frac{\alpha\sqrt{n}}{5} + \frac{1}{8}(5 - 7n + 2n^2) + O(\alpha^3), \tag{C12}$$

$$\langle\hat{n}^2\rangle = \sum_{m=0}^{\infty} m^2 P_m^{+,n} = \left(n^2 - n + \frac{1}{2}\right) + \frac{\alpha}{4}(1-2n)\sqrt{n} + \frac{\alpha^2}{8}(2n^3 - 10n^2 + 17n - 5) + O(\alpha^3). \tag{C13}$$

In order to prove that the distribution is sub-Poissonian, it is sufficient to study the sign of

$$\langle\hat{n}^2\rangle - \langle\hat{n}\rangle^2 - \langle\hat{n}\rangle = \left(\frac{3}{4} - n\right) + \frac{\alpha\sqrt{n}}{4} - \frac{\alpha^2}{16}(4n^3 - 8n^2 - 13n + 10), \tag{C14}$$

which can be straightforwardly proven to be negative in the pUSC regime, i.e., assuming that $0 \leqslant \alpha \leqslant 1/\sqrt{2(2n+1)}$. The cubic polynomial is negative when $n = 1,2$ and positive when $n \geqslant 3$. The first case can be directly checked. In the second case, $\langle\hat{n}^2\rangle - \langle\hat{n}\rangle^2 - \langle\hat{n}\rangle \leqslant (\frac{3}{4} - n) + \sqrt{\frac{n}{8(2n+1)}} \leqslant (\frac{3}{4} - n) + \frac{1}{4} < 0$, which finally proves that the photon distribution of the states $|\phi^{\mathrm{BS}}_{n,+}\rangle$ is sub-Poissonian. In order to extend it to the states $|\phi^{\mathrm{BS}}_{n,-}\rangle$, it is only necessary to apply the substitutions $\sin\frac{\theta_n}{2} \to -\cos\frac{\theta_n}{2}$ and $\cos\frac{\theta_n}{2} \to \sin\frac{\theta_n}{2}$ in Eqs. (C10) and (C11) and proceed analogously. This yields

$$\langle\hat{n}^2\rangle - \langle\hat{n}\rangle^2 - \langle\hat{n}\rangle = \left(\frac{3}{4} - n\right) - \frac{\alpha\sqrt{n}}{4} - \frac{\alpha^2}{16}(4n^3 - 8n^2 - 13n + 10), \tag{C15}$$

which is also negative for $n \geqslant 1$. This concludes the proof.

2. Perturbative DSC regime

Here, we prove that the photon distribution of the eigenstates of the QRM in the DSC regime is super-Poissonian. To achieve it, we proceed similarly to the previous subsection, assuming that in DSC the eigenstates are correctly described

by Eq. (17). It is straightforward to see that

$$\left\langle \mathrm{g},m\middle|\phi^{\mathrm{pDSC}}_{\pm,n}\right\rangle = \frac{1}{2}(\langle m|\mathcal{D}(-\alpha)|n\rangle \mp \langle m|\mathcal{D}(\alpha)|n\rangle), \tag{C16}$$

$$\left\langle \mathrm{e},m\middle|\phi^{\mathrm{pDSC}}_{\pm,n}\right\rangle = \frac{1}{2}(\langle m|\mathcal{D}(-\alpha)|n\rangle \pm \langle m|\mathcal{D}(\alpha)|n\rangle), \tag{C17}$$

where

$$\langle m|\mathcal{D}(\alpha)|n\rangle = \sqrt{\frac{m!}{n!}}e^{-\frac{1}{2}\alpha^2}\alpha^{m+n}\sum_{k=0}^{\min(n,m)}\frac{(-1)^{n-k}}{(m-k)!}\binom{n}{k}\alpha^{-2k}. \tag{C18}$$

Let us start by computing the photon distribution for $|\phi^{\mathrm{pDSC}}_{+,n}\rangle$, which means that $P_m(\phi^{\mathrm{pDSC}}_{n,+}) = |\langle \mathrm{g},m|\phi^{\mathrm{pDSC}}_{n,+}\rangle|^2 + |\langle \mathrm{e},m|\phi^{\mathrm{pDSC}}_{n,+}\rangle|^2$ is given by

$$\begin{aligned} P_m\left(\phi^{\mathrm{pDSC}}_{n,+}\right) &= \left|\sqrt{\frac{m!}{n!}}\frac{e^{-\frac{1}{2}\alpha^2}\alpha^{m+n}}{2}\sum_{k=0}^{n}\frac{(-1)^{n-k}}{(m-k)!}\binom{n}{k}\alpha^{-2k}\right|^2 \\ &\quad\times \underbrace{((1-(-1)^{m+n})^2+(1+(-1)^{m+n})^2)}_{=4} \\ &= |\langle m|\mathcal{D}(\alpha)|n\rangle)|^2. \end{aligned}$$

Taking this into account, the computation of the first and second moments is straightforward, since

$$\begin{aligned} \langle\hat{n}\rangle &= \sum_{m=0}^{\infty} m P_m^{+,n} = \sum_{m=0}^{\infty}\langle n|\mathcal{D}^\dagger(\alpha)\underbrace{|m\rangle m\langle m|}_{\hat{n}=a^\dagger a}\mathcal{D}(\alpha)|n\rangle \\ &= n+\alpha^2, \end{aligned} \tag{C19}$$

$$\begin{aligned} \langle\hat{n}^2\rangle &= \sum_{m=0}^{\infty} m^2 P_m^{+,n} = \sum_{m=0}^{\infty}\langle n|\mathcal{D}^\dagger(\alpha)\underbrace{|m\rangle m^2\langle m|}_{\hat{n}^2=(a^\dagger a)^2}\mathcal{D}(\alpha)|n\rangle \\ &= n^2+\alpha^4+\alpha^2(4n+1). \end{aligned} \tag{C20}$$

Therefore, in order to prove that the distribution is super-Poissonian for $\alpha \gtrsim g^{\times}_{\mathrm{pDSC}}/\omega$, we have to study the sign of

$$\langle\hat{n}^2\rangle - \langle\hat{n}\rangle^2 - \langle\hat{n}\rangle = n(2\alpha^2-1) > 0, \tag{C21}$$

which proves it, since α is always bigger than $1/\sqrt{2}$ in the pDSC regime (see Table I). For the case of the eigenstates $|\phi^{\mathrm{pDSC}}_{-,n}\rangle$, we only need to notice that the photon distribution is exactly the same, hence Eqs. (C18)–(C21) also hold, which concludes the proof.

APPENDIX D: CAVITY-QUBIT ENTANGLEMENT

In this Appendix, we compute the cavity-qubit entanglement via the von-Neumann entropy in the pUSC and pDSC regimes, which allows us to analytically prove the numerical observations in Sec. III.

1. Von-Neumann entropy in the pUSC regime

We have to compute the reduce density matrix for the qubit system. By using the Baker-Haussdorff-Campbell formula,

$$\begin{aligned} \mathcal{U}|\pm,n\rangle\langle\pm n|\mathcal{U}^\dagger &= |\pm,n\rangle\langle\pm n| + [\mathcal{H}(\alpha),|\pm,n\rangle\langle\pm n|] \\ &\quad + \tfrac{1}{2}[\mathcal{H}(\alpha),[\mathcal{H}(\alpha),|\pm,n\rangle\langle\pm n|]] \\ &\quad + O(\mathcal{H}(\alpha)^3), \end{aligned} \tag{D1}$$

in which $\alpha = g_0/\omega$ with $\mathcal{H}(\alpha)$ given by Eq. (C3). The reduced density matrix is obtained by tracing out the bosonic degrees of freedom, i.e., $\rho_{n,\pm} = \mathrm{Tr}_{\mathrm{cav}}(\mathcal{U}|\pm,n\rangle\langle\pm n|\mathcal{U}^\dagger)$. As usual, let us first consider the states $|+,n\rangle$. Then, the contribution to the reduced density matrix due to the first term in Eq. (D1) is

$$\begin{aligned} \rho^{(1)} &= \mathrm{Tr}_{\mathrm{cav}}(|+,n\rangle\langle+n|) \\ &= \cos^2\frac{\theta_n}{2}|e\rangle\langle e| + \sin^2\frac{\theta_n}{2}|g\rangle\langle g|. \end{aligned} \tag{D2}$$

For the second term, it is straightforward to prove that $\rho^{(2)} = \mathrm{Tr}_{\mathrm{cav}}([\mathcal{H}(\alpha),|+,n\rangle\langle+n|]) = O(\alpha^3)$, so it will not be considered.

Finally, for the third term we must only consider the influence of the Hamiltonian term $\frac{\alpha}{2}(a\sigma^- - a^\dagger\sigma^+)$, since we are working in $O(\alpha^2)$. Let us notice that the double commutator can be rewritten as $[\mathcal{H}(\alpha),[\mathcal{H}(\alpha),|\pm,n\rangle\langle\pm n|]] = \{|\pm,n\rangle\langle\pm n|,\mathcal{H}(\alpha)^2\} - 2\mathcal{H}(\alpha)|\pm,n\rangle\langle\pm n|\mathcal{H}(\alpha)$, so let us compute both terms separately. The anticommutator yields

$$\begin{aligned} &\mathrm{Tr}_{\mathrm{cav}}(\{|+,n\rangle\langle+,n|,\mathcal{H}(\alpha)^2\}) \\ &= -\frac{\alpha^2}{4}\left[(n-1)\cos^2\frac{\theta_n}{2}|\mathrm{e}\rangle\langle\mathrm{e}| + (n+1)\sin^2\frac{\theta_n}{2}|\mathrm{g}\rangle\langle\mathrm{g}|\right]. \end{aligned} \tag{D3}$$

Analogously, one obtains

$$\begin{aligned} &\mathrm{Tr}_{\mathrm{cav}}(\mathcal{H}(\alpha)|+,n\rangle\langle+,n|\mathcal{H}(\alpha)) \\ &= -\frac{\alpha^2}{4}\left[(n+1)\sin^2\frac{\theta_n}{2}|\mathrm{e}\rangle\langle\mathrm{e}| + (n-1)\cos^2\frac{\theta_n}{2}|\mathrm{g}\rangle\langle\mathrm{g}|\right], \end{aligned} \tag{D4}$$

such that the total contribution to the $\rho^{(3)}$, using that $\sin^2\frac{\theta_n}{2} = \cos^2\frac{\theta_n}{2} = \frac{1}{2} + O(\alpha)$, is given by

$$\rho^{(3)} = \frac{\alpha^2}{2}(|\mathrm{e}\rangle\langle\mathrm{e}| - |\mathrm{g}\rangle\langle\mathrm{g}|) = \frac{\alpha^2}{2}\sigma_z. \tag{D5}$$

Therefore, the total density matrices for $n > 0$ are given by

$$\begin{aligned} \rho_{n,\pm} &= \left(\frac{1}{2} \pm \frac{\alpha\sqrt{n}}{4} + \frac{\alpha^2}{4}\right)|\mathrm{e}\rangle\langle\mathrm{e}| \\ &\quad + \left(\frac{1}{2} \mp \frac{\alpha\sqrt{n}}{4} - \frac{\alpha^2}{4}\right)|\mathrm{g}\rangle\langle\mathrm{g}|. \end{aligned} \tag{D6}$$

We can see that the entanglement is maximum for $\alpha \approx 0$, as numerically observed. The von-Neumann entropy $S(\rho) = -\sum_k \lambda_k \log_2\lambda_k$, where λ_k are the eigenvalues of ρ, is

$$S(\rho_{n,\pm}) = 1 - \frac{n\alpha^2}{8} + O(\alpha^3). \tag{D7}$$

2. Von-Neumann entropy in the pDSC regime

Let us take the states describing the cavity-qubit system in the pDSC regime given by Eq. (17), and trace out the bosonic degrees of freedom,

$$\begin{aligned} &\mathrm{Tr}_{\mathrm{cav}}\left(\left|\phi^{\mathrm{pDSC}}_{\pm,n}\right\rangle\left\langle\phi^{\mathrm{pDSC}}_{\pm,n}\right|\right) \\ &= \frac{1}{2}[|+\rangle\langle+| + |-\rangle\langle-| \pm |+\rangle\langle-|\langle n|\mathcal{D}^2(-\alpha)|n\rangle \\ &\quad \pm |-\rangle\langle+|\langle n|\mathcal{D}^2(\alpha)|n\rangle]. \end{aligned} \tag{D8}$$

Therefore, the aim here is to compute $\langle n|\mathcal{D}^2(\alpha)|n\rangle = \langle n|\mathcal{D}(2\alpha)|n\rangle = \langle n|\mathcal{D}(2\alpha)\frac{(a^\dagger)^n}{\sqrt{n!}}\mathcal{D}^\dagger(2\alpha)\mathcal{D}(2\alpha)|0\rangle$. By using $\mathcal{D}(2\alpha)a^\dagger\mathcal{D}^\dagger(2\alpha) = a^\dagger - 2\alpha$ and the Newton's binomial theorem,

$$\langle n|\mathcal{D}^2(\alpha)|n\rangle = \frac{1}{\sqrt{n!}}\langle n|\sum_{k=0}^{n}\binom{n}{k}(-2\alpha)^{n-k}a^{\dagger k}|2\alpha\rangle = \sum_{k=0}^{n}\binom{n}{k}(-2\alpha)^{n-k}\frac{\langle n-k|2\alpha\rangle}{\sqrt{(n-k)!}}, \tag{D9}$$

where we have used $a^k|n\rangle = \sqrt{\frac{n!}{(n-k)!}}|n-k\rangle$. Then, employing $\langle n-k|2\alpha\rangle = e^{-2\alpha^2}\frac{(2\alpha)^{n-k}}{\sqrt{(n-k)!}}$, we have

$$\langle n|\mathcal{D}^2(\alpha)|n\rangle = e^{-2\alpha^2}\sum_{k=0}^{n}\binom{n}{k}(-1)^k\frac{(2\alpha)^{2k}}{k!} = e^{-2\alpha^2}{}_1F_1(-n,1;4\alpha^2), \tag{D10}$$

where ${}_1F_1(a,b;z)$ is the Kummer confluent hypergeometric function [71].

Therefore, the two eigenvalues of the reduced density matrix for the qubit are

$$\lambda_\pm\left(\phi^{\mathrm{pDSC}}_{\pm,n}\right) = \tfrac{1}{2}[1 \pm e^{-2\alpha^2}{}_1F_1(-n,1;4\alpha^2)]. \tag{D11}$$

Notice that the eigenvalues only depend on the quantum number n. Finally, we can compute the entropy $S = -\frac{1}{2}(1-y)\log_2(\frac{1-y}{2}) - \frac{1}{2}(1+y)\log_2(\frac{1+y}{2}) = 1 - \frac{y^2}{2} + O(y^4)$, with $y = e^{-2\alpha^2}{}_1F_1(-n,1;4\alpha^2) \ll 1$ in the pDSC region. Hence, the entropy is given by

$$S = 1 - \frac{1}{2}\underbrace{e^{-4\alpha^2}{}_1F_1^2(-n,1;4\alpha^2)}_{\leqslant\epsilon^2}, \tag{D12}$$

which exponentially tends to 1 and it is lower bounded by $S \geqslant 1 - \frac{1}{2}\epsilon^2$ in the pDSC region.

[1] I. I. Rabi, On the Process of Space Quantization, Phys. Rev. **49**, 324 (1936); Space Quantization in a Gyrating Magnetic Field, **51**, 652 (1937).

[2] D. Braak, Integrability of the Rabi Model, Phys. Rev. Lett. **107**, 100401 (2011).

[3] E. Solano, Viewpoint: The dialogue between quantum light and matter, Physics **4**, 68 (2011).

[4] A. Auffèves, D. Gerace, R. Maxime, S. Portolan, M. F. Santos, L. C. Kwek, and C. Miniatura, *Strong Light-Matter Coupling: From Atoms to Solid-State Physics* (World Scientific, Singapore, 2013).

[5] M. A. Nielsen and I. L. Chuang, *Quantum Computation and Quantum Information* (Cambridge University Press, Cambridge, 2004).

[6] G. Romero, D. Ballester, Y. M. Wang, V. Scarani, and E. Solano, Ultrafast Quantum Gates in Circuit QED, Phys. Rev. Lett. **108**, 120501 (2012).

[7] T. H. Kyaw, D. A. Herrera-Martí, E. Solano, G. Romero, and L.-C. Kwek, Creation of quantum error correcting codes in the ultrastrong coupling regime, Phys. Rev. B **91**, 064503 (2015).

[8] S. Felicetti, M. Sanz, L. Lamata, G. Romero, G. Johansson, P. Delsing, and E. Solano, Dynamical Casimir Effect Entangles Artificial Atoms, Phys. Rev. Lett. **113**, 093602 (2014).

[9] D. Z. Rossatto, S. Felicetti, H. Eneriz, E. Rico, M. Sanz, and E. Solano, Entangling polaritons via dynamical Casimir effect in circuit quantum electrodynamics, Phys. Rev. B **93**, 094514 (2016).

[10] E. T. Jaynes and F. W. Cummings, Comparison of quantum and semiclassical radiation theories with application to the beam maser, Proc. IEEE **51**, 89 (1963).

[11] C. Gerry and P. Knight, *Introductory Quantum Optics* (Cambridge University Press, New York, 2005).

[12] C. Ciuti, G. Bastard, and I. Carusotto, Quantum vacuum properties of the intersubband cavity polariton field, Phys. Rev. B **72**, 115303 (2005).

[13] J. Bourassa, J. M. Gambetta, A. A. Abdumalikov, Jr., O. Astafiev, Y. Nakamura, and A. Blais, Ultrastrong coupling regime of cavity QED with phase-biased flux qubits, Phys. Rev. A **80**, 032109 (2009).

[14] F. Beaudoin, J. M. Gambetta, and A. Blais, Dissipation and ultrastrong coupling in circuit QED, Phys. Rev. A **84**, 043832 (2011).

[15] D. Ballester, G. Romero, J. J. García-Ripoll, F. Deppe, and E. Solano, Quantum Simulation of the Ultrastrong Coupling Dynamics in Circuit QED, Phys. Rev. X **2**, 021007 (2012).

[16] J. S. Pedernales, I. Lizuain, S. Felicetti, G. Romero, L. Lamata, and E. Solano, Quantum Rabi Model with Trapped Ions, Sci. Reps. **5**, 15472 (2015).

[17] A. P. Saiko, S. A. Markevich, and R. Fedaruk, Dissipative two-level systems under ultrastrong off-resonant driving, Phys. Rev. A **93**, 063834 (2016).

[18] Y. Todorov, A. M. Andrews, R. Colombelli, S. De Liberato, C. Ciuti, P. Klang, G. Strasser, and C. Sirtori, Ultrastrong Light-Matter Coupling Regime with Polariton Dots, Phys. Rev. Lett. **105**, 196402 (2010).

[19] P. Forn-Díaz, J. Lisenfeld, D. Marcos, J. J. García-Ripoll, E. Solano, C. J. P. M. Harmans, and J. E. Mooij, Observation of the Bloch-Siegert Shift in a Qubit-Oscillator System in the Ultrastrong Coupling Regime, Phys. Rev. Lett. **105**, 237001 (2010).

[20] T. Niemczyk, F. Deppe, H. Huebl, E. P. Menzel, F. Hocke, M. J. Schwarz, J. J. García-Ripoll, D. Zueco, T. Hümmer, E. Solano, A. Marx, and R. Gross, Circuit quantum electrodynamics in the ultrastrong-coupling regime, Nat. Phys. **6**, 772 (2010).

[21] G. Scalari, C. Maissen, D. Turcinkova, D. Hagenmüller, S. De Liberato, C. Ciuti, C. Reichl, D. Schuh, W. Wegscheider, M. Beck, and J. Faist, Ultrastrong coupling of the cyclotron transition of a 2D electron gas to a THz metamaterial, Science **335**, 1323 (2012).

[22] A. A. Anappara, S. De Liberato, A. Tredicucci, C. Ciuti, G. Biasiol, L. Sorba, and F. Beltram, Signatures of the ultrastrong light-matter coupling regime, Phys. Rev. B **79**, 201303(R) (2009).

[23] G. Günter, A. A. Anappara, J. Hees, A. Sell, G. Biasiol, L. Sorba, S. De Liberato, C. Ciuti, A. Tredicucci, A. Leitenstorfer and R. Huber, Sub-cycle switch-on of ultrastrong light–matter interaction, Nature (London) **458**, 178 (2009).

[24] A. Fedorov, A. K. Feofanov, P. Macha, P. Forn-Díaz, C. J. P. M. Harmans, and J. E. Mooij, Strong Coupling of a Quantum Oscillator to a Flux Qubit at Its Symmetry Point, Phys. Rev. Lett. **105**, 060503 (2010).

[25] V. M. Muravev, I. V. Andreev, I. V. Kukushkin, S. Schmult, and W. Dietsche, Observation of hybrid plasmon-photon modes in microwave transmission of coplanar microresonators, Phys. Rev. B **83**, 075309 (2011).

[26] T. Schwartz, J. A. Hutchison, C. Genet, and T. W. Ebbesen, Reversible Switching of Ultrastrong Light-Molecule Coupling, Phys. Rev. Lett. **106**, 196405 (2011).

[27] M. Geiser, F. Castellano, G. Scalari, M. Beck, L. Nevou, and J. Faist, Ultrastrong Coupling Regime and Plasmon Polaritons in Parabolic Semiconductor Quantum Wells, Phys. Rev. Lett. **108**, 106402 (2012).

[28] M. Goryachev, W. G. Farr, D. L. Creedon, Y. Fan, M. Kostylev, and M. E. Tobar, High-Cooperativity Cavity QED with Magnons at Microwave Frequencies, Phys. Rev. Applied **2**, 054002 (2014).

[29] Q. Zhang, M. Lou, X. Li, J. L. Reno, W. Pan, J. D. Watson, M. J. Manfra, and J. Kono, Collective, coherent, and ultrastrong coupling of 2D electrons with terahertz cavity photons, Nat. Phys. **12**, 1005 (2016).

[30] Z. Chen, Y. Wang, T. Li, L. Tian, Y. Qiu, K. Inomata, F. Yoshihara, S. Han, F. Nori, J. S. Tsai, and J. Q. You, Multi-photon sideband transitions in an ultrastrongly coupled circuit quantum electrodynamics system, Phys. Rev. A (to be published), arXiv:1602.1584.

[31] N. K. Langford, R. Sagastizabal, M. Kounalakis, C. Dickel, A. Bruno, F. Luthi, D. J. Thoen, A. Endo, and L. DiCarlo, Experimentally simulating the dynamics of quantum light and matter at ultrastrong coupling, arXiv:1610.10065.

[32] J. Braumüller, M. Marthaler, A. Schneider, A. Stehli, H. Rotzinger, M. Weides, and A. V. Ustinov, Analog quantum simulation of the Rabi model in the ultra-strong coupling regime, arXiv:1611.8404.

[33] S. Ashhab and F. Nori, Qubit-oscillator systems in the ultrastrong-coupling regime and their potential for preparing nonclassical states, Phys. Rev. A **81**, 042311 (2010).

[34] P. Nataf and C. Ciuti, Protected Quantum Computation with Multiple Resonators in Ultrastrong Coupling Circuit QED, Phys. Rev. Lett. **107**, 190402 (2011).

[35] A. Ridolfo, M. Leib, S. Savasta, and M. J. Hartmann, Photon Blockade in the Ultrastrong Coupling Regime, Phys. Rev. Lett. **109**, 193602 (2012).

[36] A. Ridolfo, S. Savasta, and M. J. Hartmann, Nonclassical Radiation from Thermal Cavities in the Ultrastrong Coupling Regime, Phys. Rev. Lett. **110**, 163601 (2013).

[37] R. Stassi, A. Ridolfo, O. D. Stefano, M. J. Hartmann, and S. Savasta, Spontaneous Conversion from Virtual to Real Photons in the Ultrastrong-Coupling Regime, Phys. Rev. Lett. **110**, 243601 (2013).

[38] S. Felicetti, G. Romero, D. Rossini, R. Fazio, and E. Solano, Photon transfer in ultrastrongly coupled three-cavity arrays, Phys. Rev. A **89**, 013853 (2014).

[39] L. Garziano, R. Stassi, A. Ridolfo, O. D. Stefano, and S. Savasta, Vacuum-induced symmetry breaking in a superconducting quantum circuit, Phys. Rev. A **90**, 043817 (2014).

[40] L. Garziano, R. Stassi, V. Macrì, A. F. Kockum, S. Savasta, and F. Nori, Multiphoton quantum Rabi oscillations in ultrastrong cavity QED, Phys. Rev. A **92**, 063830 (2015).

[41] T. H. Kyaw, S. Felicetti, G. Romero, E. Solano, and L. C. Kwek, Scalable quantum memory in the ultrastrong coupling regime, Sci. Rep. **5**, 8621 (2015).

[42] S. Felicetti, T. Douce, G. Romero, P. Milman, and E. Solano, Parity-dependent state engineering and tomography in the ultrastrong coupling regime, Sci. Rep. **5**, 11818 (2015).

[43] P. Forn-Díaz, G. Romero, C. J. P. M. Harmans, E. Solano, and J. E. Mooij, Broken selection rule in the quantum Rabi model, Sci. Rep. **6**, 26720 (2016).

[44] Y. Wang, J. Zhang, C. Wu, J. Q. You, and G. Romero, Holonomic quantum computation in the ultrastrong-coupling regime of circuit QED, Phys. Rev. A **94**, 012328 (2016).

[45] A. B. Klimov and S. M. Chumakov, *A Group-Theoretical Approach to Quantum Optics* (WILEY-VCH, Weinheim, 2009).

[46] C. Maissen, G. Scalari, F. Valmorra, M. Beck, J. Faist, S. Cibella, R. Leoni, C. Reichl, C. Charpentier, and W. Wegscheider, Ultrastrong coupling in the near field of complementary split-ring resonators, Phys. Rev. B **90**, 205309 (2014).

[47] S. Gambino, M. Mazzeo, A. Genco, O. D. Stefano, S. Savasta, S. Patane, D. Ballarini, F. Mangione, G. Lerario, D. Sanvitto, and G. Gigli, Exploring light-matter interaction phenomena under ultrastrong coupling regime, ACS Photon. **1**, 1042 (2014).

[48] P. Forn-Díaz, J. J. García-Ripoll, B. Peropadre, M. A. Yurtalan, J.-L. Orgiazzi, R. Belyansky, C. M. Wilson, and A. Lupascu, Ultrastrong coupling of a single artificial atom to an electromagnetic continuum, Nat. Phys. **13**, 39 (2017).

[49] F. Yoshihara, T. Fuse, S. Ashhab, K. Kakuyanagi, S. Saito, and K. Semba, Superconducting qubit-oscillator circuit beyond the ultrastrong-coupling regime, Nat. Phys. **13**, 44 (2017).

[50] F. Yoshihara, T. Fuse, S. Ashhab, K. Kakuyanagi, S. Saito, and K. Semba, Characteristic spectra of circuit quantum electrodynamics systems from the ultrastrong to the deep strong coupling regime, Phys. Rev. A **95**, 053824 (2017).

[51] J. Casanova, G. Romero, I. Lizuain, J. J. García-Ripoll, and E. Solano, Deep Strong Coupling Regime of the Jaynes-Cummings Model, Phys. Rev. Lett. **105**, 263603 (2010).

[52] S. De Liberato, Light-Matter Decoupling in the Deep Strong Coupling Regime: The Breakdown of the Purcell Effect, Phys. Rev. Lett. **112**, 016401 (2014).

[53] I. D. Feranchuk, I. I. Komarov, and A. P. Ulyanekov, Two-level system in a one-mode quantum field: numerical solution on the basis of the operator method, J. Phys. A **29**, 4035 (1996).

[54] E. K. Irish, J. Gea-Banacloche, I. Martin, and K. C. Schwab, Dynamics of a two-level system strongly coupled to a high-frequency quantum oscillator, Phys. Rev. B **72**, 195410 (2005).

[55] E. K. Irish, Generalized Rotating-Wave Approximation for Arbitrarily Large Coupling, Phys. Rev. Lett. **99**, 173601 (2007).

[56] L. Yu, S. Zhu, Q. Liang, G. Chen, and S. Jia, Analytical solutions for the Rabi model, Phys. Rev. A **86**, 015803 (2012).

[57] V. V. Albert, G. D. Scholes, and P. Brumer, Symmetric rotating-wave approximation for the generalized single-mode spin-boson system, Phys. Rev. A **84**, 042110 (2011).

[58] T. Liu, K.-L. Wang, and M. Feng, The generalized analytical approximation to the solution of the single-mode spin-boson model without rotating-wave approximation, Europhys. Lett. **86**, 54003 (2009).

[59] M. Amniat-Talab, S. Guérin, and H. R. Jauslin, Quantum averaging and resonances: Two-level atom in a one-mode quantized field, J. Math. Phys. **46**, 042311 (2005).

[60] R. Graham and M. Hohnerbach, Two-state system coupled to a boson mode: quantum dynamics and classical approximations, Z. Phys. B **57**, 233 (1984).

[61] F. A. Wolf, F. Vallone, G. Romero, M. Kollar, E. Solano, and D. Braak, Dynamical correlation functions and the quantum Rabi model, Phys. Rev. A **87**, 023835 (2013).

[62] A. Vukics, T. Grießer, and P. Domokos, Fundamental limitation of ultrastrong coupling between light and atoms, Phys. Rev. A **92**, 043835 (2015).

[63] T. Jaako, Z.-L. Xiang, J. J. García-Ripoll, and P. Rabl, Ultrastrong-coupling phenomena beyond the Dicke model, Phys. Rev. A **94**, 033850 (2016).

[64] P. Nataf and C. Ciuti, No-go theorem for superradiant quantum phase transitions in cavity QED and counter-example in circuit QED, Nat. Comm. **1**, 72 (2010).

[65] O. Viehmann, J. von Delft, and F. Marquardt, Superradiant Phase Transitions and the Standard Description of Circuit QED, Phys. Rev. Lett. **107**, 113602 (2011).

[66] C. Ciuti and P. Nataf, Comment on "Superradiant Phase Transitions and the Standard Description of Circuit QED", Phys. Rev. Lett. **109**, 179301 (2012).

[67] M. Bamba, K. Inomata, and Y. Nakamura, Super-Radiant Phase Transition in Superconducting Circuit in Thermal Equilibrium, Phys. Rev. Lett. **117**, 173601 (2016).

[68] Z.-J. Ying, M. Liu, H.-G. Luo, H.-Q. Lin, and J. Q. You, Ground-state phase diagram of the quantum Rabi model, Phys. Rev. A **92**, 053823 (2015).

[69] We numerically found that the fidelity between the BS eigenstates and the Rabi eigenstates is greater than 99% before the Juddian points.

[70] M.-J. Hwang, R. Puebla, and M. B. Plenio, Quantum Phase Transition and Universal Dynamics in the Rabi Model, Phys. Rev. Lett. **115**, 180404 (2015).

[71] in *NIST Handbook of Mathematical Functions*, edited by F. W. J. Olver, D. W. Lozier, R. F. Boisvert, and C. W. Clark (Cambridge University Press, New York, 2010), p. 328.